PAPER

Check for updates

Valorization of cash crop waste into a decomposable nanocellulose adsorbent matrix through bacterial cell factories for the management of agricultural runoff contaminants

Bendangtula Walling,[a] Pranjal Bharali, [ID] *[a] D. Ramachandran,[b]
Viswanathan Kanagasabai,[b] Swapnali Hazarika,[c] Nipu Dutta,[d]
Panneerselvam Vengatesh,[b] M. Thangam,[b] Shiva Aley Acharjee[a]
and Vinita Vishwakarma[e]

Agricultural runoff remains a pressing environmental concern, driven by the widespread use of herbicides and antibiotics in farming systems. In response, this study introduces a dual-purpose strategy that not only mitigates farming pollutants but also valorizes agro-industrial waste. Waste sugarcane molasses (WSM), an often-overlooked by-product, was repurposed as a sole carbon source for cultivating *Komagataeibacter saccharivorans* NUWB1, yielding 12.68 g L^{-1} bacterial nanocellulose (BNC) with superior structural and functional properties. Experimental findings revealed that BNC yield was strongly influenced by the surface-to-volume (S/V) ratio of the culture system, with higher S/V enhancing oxygen availability and biosynthesis efficiency. The resulting BNC featured a mesoporous nanofibrous architecture with a BET surface area of 89.42 m^2 g^{-1}, a crystallinity index of 88%, and demonstrated good thermal stability. As an eco-benign adsorbent, BNC achieved removal efficiencies exceeding 96% for tetracycline (TC) and 2,4-dichlorophenoxyacetic acid (2,4-D), fitting the Langmuir isotherm and pseudo-second-order kinetic models, and the material maintained its adsorption efficacy over five regeneration cycles. Biodegradation studies showed over 69% disintegration within 21 days under natural soil conditions. These outcomes highlight a circular bioeconomy model where waste becomes a resource, offering a scalable and biodegradable platform for pollutant remediation.

1. Introduction

Sugarcane (*Saccharum officinarum* L.) is a crucial crop for producing sugar, jaggery, cattle feed, and energy sources like fuels. Over 110 nations rely on sugarcane cultivation to produce refined sugar, unrefined raw white sugar, and unrefined brown sugar (jaggery) for direct consumption. India is the second-largest producer of sugarcane globally, after Brazil.[1] Sugarcane molasses (MO) is a secondary product obtained during the production or purification of sugar from sugarcane.[2] It is a thick, dark, bitter liquid left after sugar crystallization, rich in minerals, commonly used as cattle feed or by local brewers. Due to its high volume, acidity, and complex composition, untreated molasses can cause significant water pollution. However, it is non-toxic, biodegradable, and rich in organic matter and trace elements, making it a valuable raw material for composting fertilizers. In terms of nutritional and economic value, this waste can be utilized to create enhanced products through chemical and biotechnological methods.[3,4]

Environmental pollution has long been a significant issue and continues to be a major cause of illness and death worldwide. Industrial molasses waste stands out as a major contributor to soil degradation. Its continued release harms soil fertility, endangers human health, and disrupts the natural environment.[5] In the late 1980s, the concept of "Zero discharge" began to gain importance in industries due to growing environmental awareness. This concept focuses on preventing waste discharges from industrial factories into the natural environment and instead promotes the recycling and reusing of all types of treated waste. Additionally, it aims to reduce air emissions and toxicity levels.[6] Recently, numerous strategies and

[a]*Applied Environmental Microbial Biotechnology Laboratory, Department of Environmental Science, Nagaland University, Lumami, Zunheboto-798627, Nagaland, India. E-mail: prangenetu@gmail.com*

[b]*Centre for Nanoscience & Nanotechnology, Sathyabama Institute of Science and Technology, Jeppiaar Nagar, Rajiv Gandhi Road, Chennai-600119, Tamil Nadu, India*

[c]*Chemical Engineering Group, CSIR-North East Institute of Science & Technology, Jorhat-785006, Assam, India*

[d]*Department of Chemical Science, Tezpur University, Napaam, Tezpur-784028, Assam, India*

[e]*Centre for Nanoscience and Nanotechnology, Galgotias University, Greater Noida, NCR Delhi, India*

technologies have emerged to repurpose industrial discharge, aiming to streamline the treatment process and transform effluent into valuable products.[7] One such approach involves using the effluent as a source of nutrients, which allows the microorganisms to break down the organic carbon within and proliferate. This serves dual purposes: reducing the organic load that requires further treatment and cultivating microorganisms that can produce valuable compounds like biopolymers. With this approach in mind, the current study focuses on repurposing waste from jaggery production to generate Bacterial Nano Cellulose (BNC) using the isolated bacterium *Komagataeibacter saccharivorans* NUWB1. Waste sugarcane molasses can be employed as an alternative carbon source to glucose, combined with other ingredients of Hestrin–Schramm medium. BNC is a biopolymer characterized by its high polymerization degree, purity, biocompatibility, biodegradability, crystallinity, and exceptional mechanical properties. These attributes make BNC a viable substitute for cellulose obtained from plants and a superior material for applications in the food sector, medicine, and environmental remediation.[8,9]

In parallel to the production of BNC using the waste sugarcane molasses, we will also be studying its efficacy in the adsorption of herbicides and antibiotics used in agriculture. The Green Revolution, initiated in the mid-20th century, transformed global agriculture with the introduction of high-yield crop varieties, synthetic fertilizers, and advanced irrigation methods. While it significantly boosted agricultural productivity and alleviated food insecurity, the widespread adoption of these technologies also intensified reliance on pesticides. Pesticides became crucial for protecting high-yield crops from pests and diseases, ensuring maximum productivity. However, concerns have since emerged over the environmental and health impacts of pesticide overuse. The Green Revolution's legacy includes enhanced food production and mitigating pesticide-related risks through sustainable agricultural practices and integrated pest management strategies.[10] This research study investigates the use of BNC for managing agricultural runoff contaminants, particularly focusing on the herbicide 2,4-dichlorophenoxyacetic acid (2,4-D), which is commonly applied to control broadleaf weeds in agricultural and garden settings. The International Agency for Research on Cancer categorizes 2,4-D as a potential carcinogen and mutagen, and it is also recognized as an endocrine-disrupting chemical.[11] The World Health Organization (WHO) established 70 $\mu g\ L^{-1}$ as the maximum permissible concentration of 2,4-D in drinking water, which is considered safe for consumption.[12] Effective methods for removing 2,4-D are crucial for maintaining a secure environment, considering its extensive use and high-water mobility, and persistence. Adsorptive removal of 2,4-D using appropriate adsorbents is considered one of the most effective approaches due to its simplicity, low cost, and mild operating conditions.[13] Another type of pollutant is tetracycline (TC), a common antibiotic extensively used in medicine, animal husbandry, and farming.[14] Reports indicate that about 90% of TCs supplied to animals are eliminated and discharged into the environment through urine or faeces. Consequently, diverse agricultural methods

employing manure or alternative trash as fertilizers may intensify the pollution of tetracyclines in arable land.[15,16] This results in a significant quantity of inadequately eliminated tetracycline entering aquatic ecosystems. TC contamination results in the mortality of aquatic organisms lacking resistance to this antibiotic. By altering natural balances and affecting biological community structures, this pollution affects human society and the entire food chain 17. Therefore, the present study aims to valorize waste sugarcane molasses as a low-cost carbon source for the production of BNC using a native strain, *Komagataeibacter saccharivorans* NUWB1, selected through systematic preliminary screening. The study further investigates the physicochemical properties of the produced BNC and evaluates its effectiveness as a biodegradable adsorbent for the removal of agricultural runoff contaminants, specifically 2,4-dichlorophenoxyacetic acid (2,4-D) and tetracycline (TC). In addition to adsorption performance, the work provides a comprehensive assessment of adsorption kinetics, equilibrium isotherms, regeneration efficiency, and biodegradability, thereby offering insights into both functional performance and end-of-life environmental fate of the BNC adsorbent.

2. Materials and methods

2.1. Chemicals and bacterial strain

All the reagents used in the present study were of analytical grade and obtained from Hi Media, India. The Hestrin–Schramm (HS) medium consisted of yeast extract (5 g L^{-1}), peptone (5 g L^{-1}), disodium hydrogen phosphate (2.7 g L^{-1}), and citric acid (1.15 g L^{-1}). 2,4-dichlorophenoxyacetic acid (2,4-D; analytical grade) was obtained from HiMedia Laboratories, India, while tetracycline hydrochloride (TC; analytical grade) was procured from Tokyo Chemical Industry (TCI), India, and used as received in the adsorption experiments. A known bacterium, *Komagataeibacter saccharivorans* NUWB1 with accession number ON764227, which was formerly isolated from a decomposed apple, was employed in the current study.

2.2. Preparation of a carbon source from waste sugarcane molasses (WSM)

WSM Fig. 1 was sourced from Tezpur, Assam, India. To eliminate particulate matter, it was first filtered and then centrifuged at 10 000 rpm for 10 minutes. The resulting supernatant was carefully collected and further purified using Whatman No. 41 filter paper. This clarified supernatant of WSM was analyzed using high-performance liquid chromatography (HPLC) (PerkinElmer) operated in isocratic mode. to identify the sugar content, with glucose, sucrose, and fructose serving as reference standards. The analysis was carried out using a Phenomenex NH_2 column with acetonitrile:water (75 : 25, v/v) as the mobile phase at a flow rate of 1.0 mL min^{-1}. The column oven temperature was maintained at 40 °C, and detection was performed using a refractive index (RI) detector. Identification and quantification of individual sugars were achieved by comparing retention times with those of known sugar standards. The

Fig. 1 Waste sugarcane molasses.

chemical characterization of WSM in the present study focused on its fermentable sugar composition, as these sugars constitute the primary carbon source governing BNC biosynthesis. Although WSM is a complex agro-industrial by-product that may also contain minerals, organic acids, and other minor constituents, detailed profiling of these components was beyond the scope of this study. To minimize compositional variability, the WSM obtained from a single source was used throughout the experiments, and clarification pretreatment was employed to remove suspended particulates prior to fermentation.

2.3. Media and BNC production

In this study, we utilized the HS culture medium to effectively produce BNC. We replaced glucose with 2 mL syrup of waste sugarcane molasses WSM while maintaining all other constituents of HS in 100 mL of distilled water. The pH of the growth medium was maintained at 6 by using 0.1 N HCl to get the best possible growth conditions.[18,19] The bacterial inoculum was prepared by cultivating *Komagataeibacter saccharivorans* NUWB1 in Hestrin–Schramm (HS) medium under static conditions until the exponential growth phase. An inoculum volume of 10% (v/v) of the actively growing culture was used to inoculate the production medium. BNC synthesis was carried out under static culture conditions at 30 °C, without agitation, using cotton-plugged conical flasks. Oxygen availability was maintained through passive diffusion from the flask headspace, allowing cellulose pellicle formation at the air–liquid interface, which is characteristic of static BNC production systems. The effect of various percentages of WSM syrup (0.5, 1, 1.5, 2, 2.5, and 3% w/v) on the production of BNC was investigated. The effect of culture medium surface area (S), depth (L), and volume (V) on the yield of BNC was also observed. To have a varied surface area, different sizes of beakers (500 mL and 250 mL)

were used that contained 100 mL, 200 mL, and 300 mL of media.

2.4. Harvesting and purification of BNC

The appearance of a gel-like pellicle formed at the air-liquid interface of the culture medium indicated the production of BNC.[20] The resulting pellicles were collected and thoroughly rinsed with distilled water to remove any remaining media components and microbial traces. Subsequently, the BNC underwent an alkali purification process, following the method described by Walling *et al.*[21]

2.5. Physicochemical characterization of the BNC film

2.5.1. Field emission scanning electron microscopy (FE-SEM) analysis. The BNC film, after purification and drying, was carefully mounted and gold-coated to prepare it for the analysis. Gold sputtering was performed to enhance surface conductivity and prevent charging effects during imaging, thereby ensuring high-resolution image capture. The surface morphology and structural characteristics were observed using a Carl Zeiss Supra-55 FESEM operated at an accelerating voltage of 5 kV.

2.5.2. Energy dispersive X-ray spectroscopy (EDX) analysis. To determine the elemental composition of the BNC film (expressed in weight percent, wt%), EDX analysis was carried out. This was performed using the point ID and mapping features of the Carl Zeiss Supra-55 FESEM (Germany). The samples were dried and coated with a conductive layer to mitigate charging during analysis. The instrument was operated under high vacuum with an accelerating voltage of 5 kV to optimize X-ray generation and elemental detection.

2.5.3. Fourier transform infrared spectroscopy (FTIR). The BNC's functional groups were identified using a FTIR (Spectrum Two, PerkinElmer). The films in the form of a thin transparent film was processed and dried, then ground into powder, and mixed with KBr before being pressed into ultra-thin pellets. The cellulose film's FTIR spectra were acquired in the 4000–400 cm^{-1} scan range with an accumulation of 32 scans, resolution of 4 cm^{-1}, and interval of 0.5 cm^{-1}.

2.5.4. Thermogravimetric analysis (TGA). The thermal stability and decomposition behavior of the BNC film were evaluated using TGA on a PerkinElmer STA 600 analyzer. Approximately 5–10 mg of sample was placed in an alumina crucible, and an empty crucible served as the reference. The analysis was conducted from ambient temperature to 700 °C at a heating rate of 20 °C min^{-1} under a nitrogen flow of 100 mL min^{-1}.

2.5.5. X-ray diffraction (XRD) analysis. XRD analysis was performed using a RIGAKU ULTIMA IV diffractometer (Japan) with Cu-Kα radiation (λ = 1.5406 Å). The instrument was operated at 40 kV and 30 mA. Data were collected at a scanning rate of 4°/min over a 2θ range of 10° to 50° to study the crystalline structure of the BNC film.

2.5.6. Brunauer–Emmett–Teller (BET) surface area analysis. The specific surface area and pore size distribution of the BNC were analyzed using BET nitrogen adsorption–desorption

isotherm measurements, conducted at liquid nitrogen temperature (-196 °C) on a Quantachrome instrument. Prior to analysis, the samples were degassed under vacuum at 150 °C for 4–5 hours to remove adsorbed gases and moisture.

2.5.7. Zeta potential analysis. Zeta potential measurements were carried out using a ZetaSizer Nano ZS (Malvern Instruments, Nano ZS 2000) to assess the surface charge characteristics of the BNC-BiVO$_4$ suspension. The sample was diluted to 0.01 wt% with deionized water, homogenized using a high-speed homogenizer at 13 000 rpm for 10 minutes, and subjected to sonication. Each measurement was repeated three times at 25 °C for accuracy.

2.6. Batch adsorption study

Batch adsorption experiments were conducted to assess the uptake of 2,4-D and TC. In these studies, BNC was added to Erlenmeyer flasks containing solutions with defined initial concentrations of each pollutant. All adsorption experiments were conducted on a mass basis using precisely weighed BNC films; the physical dimensions of individual film pieces were not fixed, as adsorption performance was normalized with respect to adsorbent mass. The adsorption experiments were performed under ambient laboratory conditions without sterilization, as the study focused on physicochemical adsorption mechanisms rather than microbial activity. These mixtures were then agitated at controlled temperatures for a specified duration. To understand the adsorption dynamics, key experimental factors including the dosage of the adsorbent, the initial pollutant concentration, the contact time, the pH of the solution, and the temperature were systematically varied. Specifically, the adsorbent dose was varied from 0.1 to 0.6 g, the initial pollutant concentration from 10 to 60 mg L^{-1}, the solution pH from 3 to 10, the contact time from 20 to 140 min, and the temperature from 298 K to 328 K. The concentrations of 2,4-D and TC in the solutions, both pre-and post-adsorption, were measured using a UV–visible spectrophotometer (Shimadzu, Japan) at wavelengths of 282 nm for 2,4-D and 357 nm for TC. Each experiment was executed in triplicate under similar conditions, and the results were recorded as averages. The pollutant quantity adsorbed per gram of BNC (q_e) and the removal efficiency (R%) from the solutions were determined using specific equations.

$$\text{Removal efficiency}(\%) = \frac{C_0 - C_e}{C_0} \times 10 \quad (1)$$

$$q_e = \frac{(C_0 - C_e)}{m} \times V \quad (2)$$

where C_0 is the concentration of the initial pollutant (mg L^{-1}), C_e is the equilibrium concentration of the pollutant, m represents the mass (g) of the adsorbent, and V(L) represents the volume of the adsorbate solution.

2.7. Studies on the biodegradability of BNC

Small BNC film samples, each measuring 2 cm by 1 cm with a thickness of 1 mm, were arranged. Soil was collected from the university campus, Lumami, India, positioned at 94°27′24.98″ E and 26°13′5.06″ N. This soil was then placed into a wooden box (dimensions: 29.5″ in length, 53.5″ in width, and 13″ in height) equipped with drainage holes at the base. Over three weeks, the samples were buried 10 cm deep in soil with a pH of 6.8, while 20 mL of water was sprinkled daily to keep the soil moist. Each week, the samples were gently taken out, rinsed with distilled water, and oven-dried at 50 °C until the weight is stable. Finally, the weight and degradation percentage were determined following the method by Walling et al.[21]

$$\text{Biodegradation}\% = \frac{(W_1 - W_2)}{W_1} \times 100 \quad (3)$$

Here, W_1 signifies the initial weight of the film, and W_2 signifies its final weight after degradation.

3 Results and discussion

3.1. Sugar composition of WSM

HPLC analysis revealed that the main sugars present in the WSM were glucose, sucrose, and fructose Fig. 2, highlighting the substrate's suitability for BNC biosynthesis. The chromatogram distinctly displays three peaks corresponding to sucrose, glucose, and fructose, with their concentrations quantified using standard references. Among these, glucose exhibits the highest concentration, with a mean % assay of 5.13%, followed by fructose at 4.91% and sucrose at 4.63%. The low % RSD (Relative Standard Deviation) values for standards and samples highlight the precision and reproducibility of the analysis. These results affirm glucose as the dominant sugar, highlighting its essential function as a carbon source. Our results are consistent with previous studies reported by Xu et al.[22] and Chikhoune et al.,[23] which described that sugarcane molasses contain significant sucrose, glucose, and fructose levels.

3.2. Effect of carbon source on BNC production

BNC was synthesized using *K. saccharivorans* NUWB1, with WSM replacing glucose as the sole carbon source in HS medium. As shown in Fig. 3a, a 2% (w/v) WSM concentration yielded the highest BNC production, while higher levels hindered growth due to pellicle thickening at the air–liquid interface, which restricted nutrient diffusion. The expanding pellicle limited nutrient access for surface microbes and further deprived those beneath it, reducing BNC yield. Thus, 2% WSM was chosen for further experiments conducted under static conditions at 30 °C and pH 6 over 14 days.

No pellicle formed on day one; by day three, a thin layer appeared at the interface, marking the onset of BNC synthesis. The pellicle thickened over time, demonstrating effective WSM utilization by *K. saccharivorans* Fig. 3b. After 14 days, the pellicle was harvested and treated with NaOH, converting it from pale yellow to a whitish, jelly-like film Fig. 3c. Following washing and drying at 50 °C, a stable BNC yield of 12.68 g L^{-1} was achieved, confirming WSM as a sustainable carbon source. It is noted that this study did not involve a direct, side-by-side comparison with
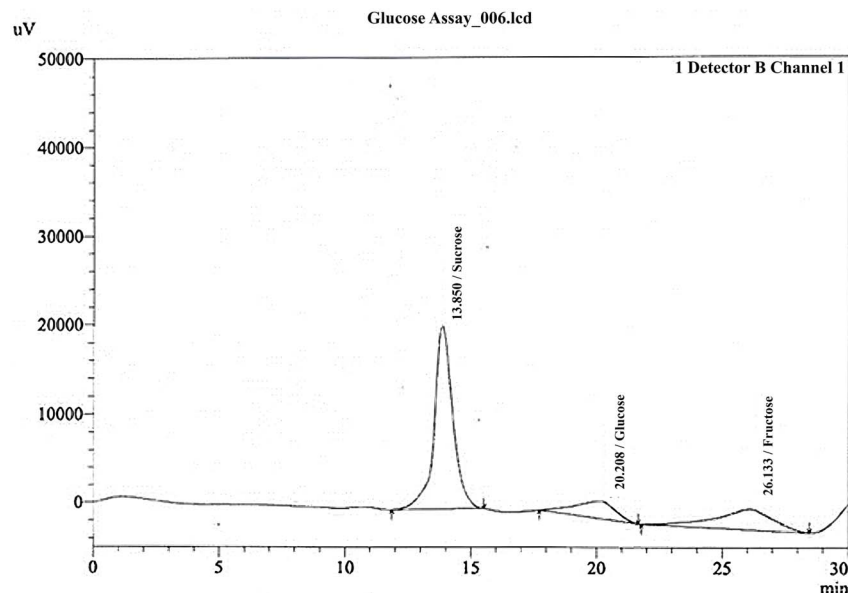
Fig. 2 HPLC chromatogram showing the presence of glucose, fructose, and sucrose in WSM.

glucose-derived BNC under identical experimental conditions; therefore, the observed performance is interpreted within the scope of evaluating the feasibility of waste sugarcane molasses as an alternative carbon source rather than attributing differences exclusively to the substrate. These findings align with previous research demonstrating WSM's potential to enhance BNC production and reduce costs. For instance, *Komagataeibacter xylinus* achieved a yield of 11.9 g L^{-1} using molasses, which was 1.6 times higher than yields from traditional media, while lowering medium costs by approximately 2.8-fold.[24] Another study reported optimized conditions that produced 7.5 g L^{-1} of BNC with molasses, surpassing yields obtained from synthetic media.[25] Although molasses offers these benefits, its variable composition can impact the consistency of BNC properties, highlighting the need for further optimization to ensure uniform quality across production batches. In this context, the BNC yield obtained in the present study (12.68 g L^{-1}) using *Komagataeibacter saccharivorans* NUWB1 and untreated waste sugarcane molasses is comparable to or higher than yields reported for other *Komagataeibacter* strains, such as *Komagataeibacter xylinus*, grown on molasses-based or agro-waste substrates under static culture conditions.[24,25] The consistent high-yield performance of NUWB1 on untreated molasses highlights its robustness and suitability for sustainable and scalable BNC production.

Optimizing the production of BNC in static cultures relies significantly on effective aeration, which is influenced by the surface-to-volume (S/V) ratio and the depth of the culture medium. In this study, we utilized two different beaker sizes: one with a volume of 500 mL and a fermentation surface area of
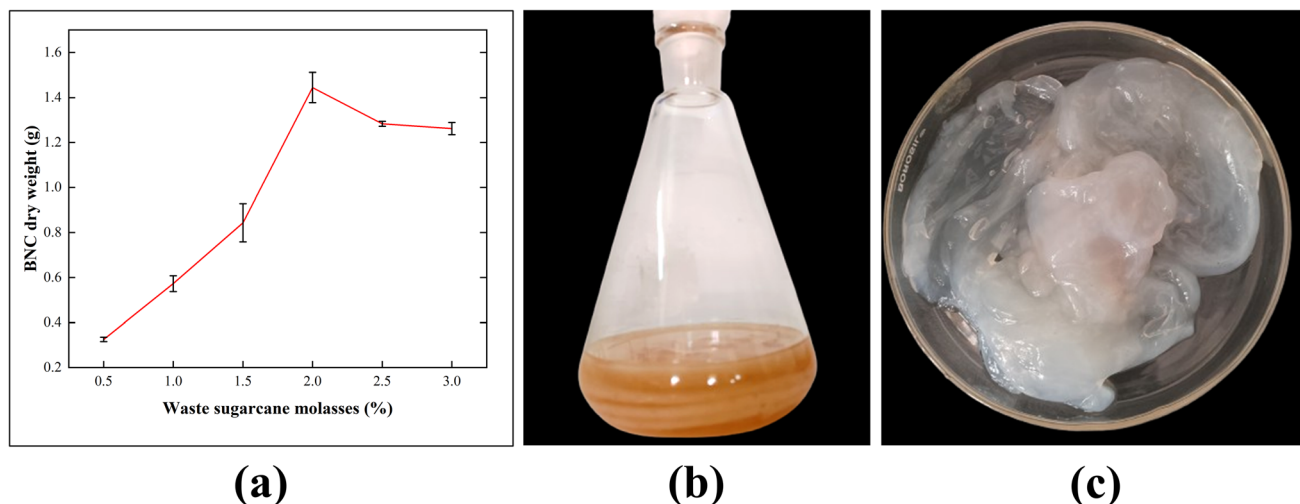

Fig. 3 (a) Influence of varying WSM concentrations on BNC biosynthesis, (b) production of BNC, and (c) BNC after purification.
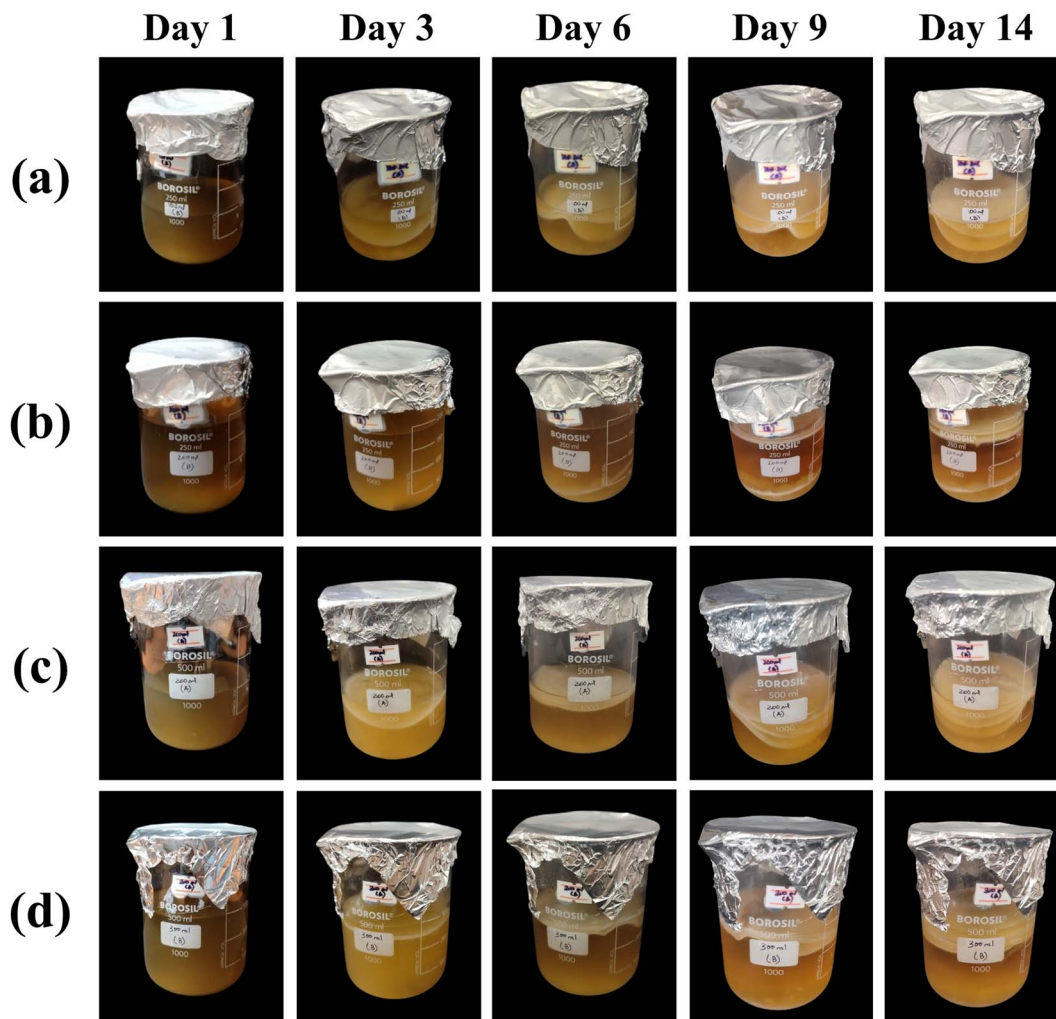
Fig. 4 Biosynthesis of BNC (a) 100 mL culture media in 250 mL beaker, (b) 200 mL culture media in 250 mL beaker, (c) 200 mL culture media in 500 mL beaker, and (d) 300 mL culture media in 500 mL beaker.

approximately 349 cm^2, and another with a volume of 250 mL and a surface area of about 220 cm^2 Fig. 4. Each beaker type was prepared with triplicate samples, filled with culture medium, and incubated statically at 30 °C. The results exhibited a positive correlation between BNC production and increased media depth, facilitating better aeration at the air-liquid interface (Table 1). Conversely, the 250 mL beaker, which held 200 mL of broth, yielded lower amounts of BNC due to its smaller air-liquid interface, restricting aeration and thereby limiting the oxygen needed for optimal BNC synthesis. Although BNC production began on the 3rd day, the resulting pellicle was thinner and less abundant compared to that produced in the 250 mL beaker containing 100 mL of media, which provided a more favourable surface area for oxygen diffusion. Previous studies, including those by Ruka et al.[26] and Walling et al.,[27] support these findings, indicating that larger media volumes improve BNC yields by ensuring nutrient availability and expanding the air-liquid interface. Moreover, controlling additional environmental factors such as temperature, pH, and inoculum density can further enhance BNC yields by promoting both bacterial growth and cellulose production.

Table 1 Comparison of BNC production in different beaker types and broth volumes

Volume of the beaker	Volume of the culture media (ml)	Surface area (cm^2)	Depth (cm)	S/V ratio (cm^{-1})	Production of BNC (g)
500 mL	300	349	6.2	1.16	3.279 ± 0.023
500 mL	200	349	4.1	1.7	3.085 ± 0.09
250 mL	200	220	5.6	1.1	1.621 ± 0.014
250 mL	100	220	3.2	2.2	1.77 ± 0.063

3.3. Physicochemical characterization

FE-SEM was used to assess the BNC surface structure. Fig. 5a demonstrates that the cellulose fibrils were firmly packed and intertwined with very few gaps between them, forming a continuous, compact three-dimensional network. The fibres displayed a ribbon-like, entangled structure, resulting in a porous architecture with few voids. This structure suggests that the fibre formation is of high quality and uniform, which is crucial for applications such as filtration, biomedical scaffolds, and biocomposites. The interconnected fibrillar network and surface texture indicate successful bacterial cellulose synthesis and self-assembly. These results are consistent with earlier studies that observed similar nanofibrous network structures.[27,28]

Fig. 5b shows the EDX spectrum of BNC derived from WSM, with highly dispersed elements, wherein mainly carbon and oxygen are dominating elements, being constituents of cellulose. The identification of additional elements, including sodium (Na), phosphorus (P), magnesium (Mg), calcium (Ca) and chlorine (Cl), indicates that the BNC not only retains the essential structural features of cellulose but also incorporates various inorganic elements which is expected to be connected with WSM. The EDX spectra revealed Na which was used in the purification of BNC through NaOH solution. Ca and Mg are major nutrients and play significant roles in plant physiological processes including photosynthesis, metabolism of carbohydrates, formation of nucleic acids, and chlorophyll. These elements are also involved in the actual formation of cell walls.

Interestingly, role of Ca includes participating in the process of nutrient absorption in plants through their roots, regulating of hydrogen ion concentration, and thus impacting soil acidity. These interactions are essential for the normal functioning of the plant growth meristem and influence the uptake of the other nutrients, notably phosphorus.[29] The detection of Cl, although not directly related to plant nutrition, may be attributed to environmental exposure, such as residual salts present in the soil or water associated with the raw material.[27]

The FTIR spectrum of BNC harvested from HS media supplemented with WSM as the carbon source reveal several key absorption peaks Fig. 5c. Specifically, the peaks at 3442, 2837, 1638, and 1424 cm^{-1} represents the different molecular vibrations: the stretching of hydroxyl groups, CH_2 stretching vibration, C–O–H bending of absorbed water, and C–H bending vibration, respectively. These peaks are consistent with the typical functional groups associated with cellulose, as stated in previous studies.[30] Interestingly, the media composition's impact on the chemical structure of BNC appears to be minimal, as no significant changes in the chemical functional groups were detected. This indicates that the type of cellulose produced remains consistent regardless of the variations in the culture media. Consequently, the chemical composition of BNC is largely unaffected regardless of the culture media used, reinforcing the identification of the specimens as cellulose.

Thermal stability of the BNC samples and degradation pattern as specified by the TGA are very important parameters in understanding the suitability of these samples for numerous
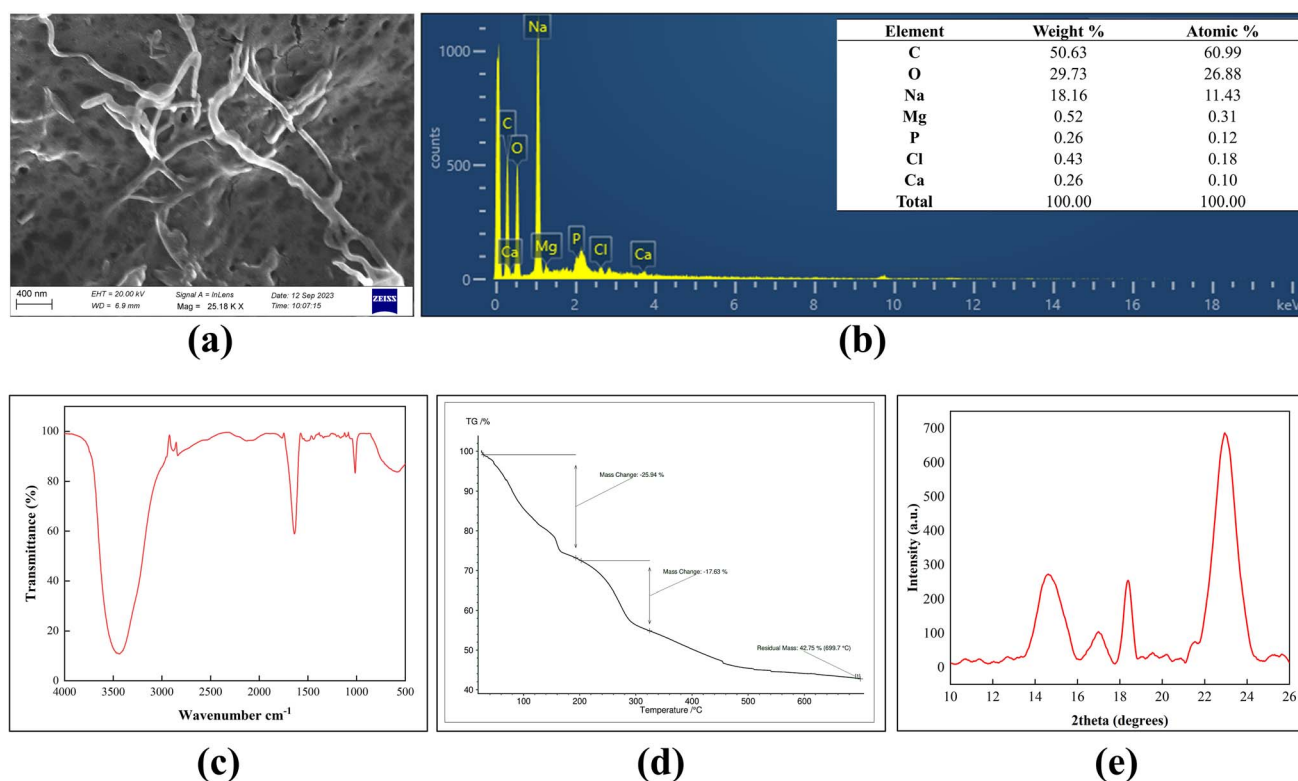

Element	Weight %	Atomic %
C	50.63	60.99
O	29.73	26.88
Na	18.16	11.43
Mg	0.52	0.31
P	0.26	0.12
Cl	0.43	0.18
Ca	0.26	0.10
Total	100.00	100.00

Fig. 5 (a) FE-SEM micrograph (Magnification = 25.18 kX; scale bar = 400 nm), (b) EDX, (c) FTIR spectrum, (d) thermogram, and (e) XRD profile of the obtained BNC.

applications particularly in regions exposing the samples to higher temperatures. As can be seen from the TGA graphs Fig. 5d, a majority of the mass loss occurs during its ascent temperature within two distinctive mass loss events. The first major mass loss with initial temperature ranged from room temperature to 180 °C which accounted for 25.94% of the initial mass, is possibly due to either moisture evaporation or any low-molecular-weight constituents, such as that of free water or other volatile organic compounds created within the nano-cellulose samples, are evaporated out during this point of nanocellulose degradation. This initial degradation phase is then followed by a distinct second stage with mass loss (17.63%), which is likely the decomposition of cellulose structure parts, associated with cellulose chains depolymerization and vaporizing smaller organic molecules.[31] The remaining residue at 699.7 °C, around 42.75%, suggests that the BNC is thermally stable, likely due to its crystalline cellulose content or carbonaceous residue formed during pyrolysis.[18,32] The high residual mass indicates excellent thermal stability, suggesting that BNC can maintain its structure under high-temperature

conditions. This characteristic may be beneficial for reinforcing polymers or serving as a component in bio-composite materials. The demonstrated thermal stability enhances BNC's potential for applications where resistance to thermal degradation is crucial, such as in electronics and bi-ocomposites. This makes BNC a versatile material for sustainable product design and advanced manufacturing applications.

The crystalline structure and type of cellulose produced by the bacterial strain can be determined using XRD analysis Fig. 5e. The peaks recorded for the BNC sample are at 2θ values of 14.71°, 17.18°, and 22.92°; these correspond to the cellulose lattice planes of the (100), (010), and (110), respectively, which indicate that it is cellulose Iα-the typical cellulose in BNC.[33] This form of cellulose Iα consists of parallel $(1 \rightarrow 4)$ linked chains, featuring intermolecular hydrogen bonds and a progressive shear along the chain axis, stabilized by van der Waals forces in a triclinic lattice structure.[34] The calculated d-spacing values and dominant crystalline allomorph are summarized in Table 2, which clearly shows an abundance of the Iα variant.[35] The strain produces BNC with a crystallinity index of 88% according to the

Table 2 Values of d-spacing and the dominant allomorph of BNC biosynthesized using WSM

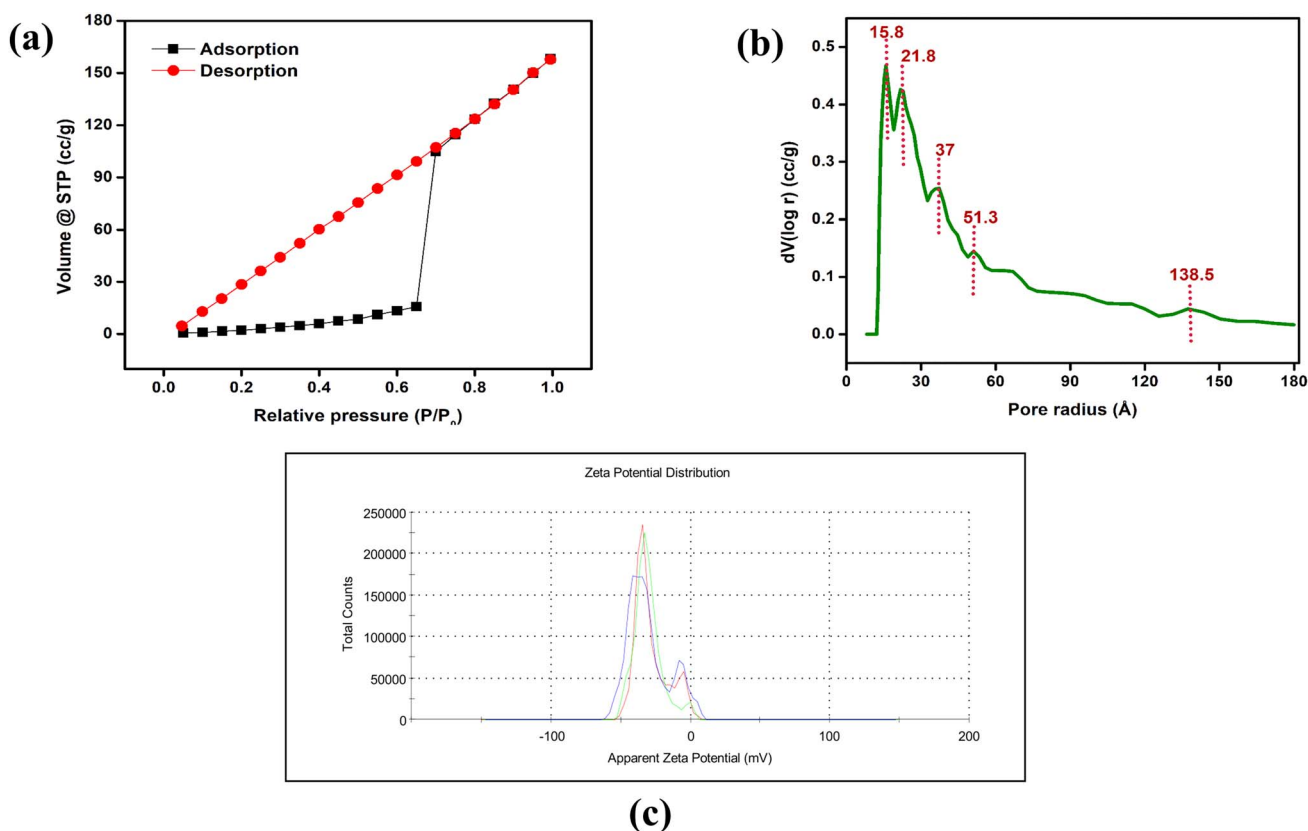| Bacterium	Carbon substrate	d- Spacing (nm)			Dominant allomorph
		d-1	d-2	d-3	
K. saccharivorans NUWB1	WSM	0.601	0.515	0.385	Iα

Fig. 6 (a) N$_2$ adsorption–desorption isotherm curve, (b) distribution graphs of pore size, and (c) zeta Potential.

Segal equation, referring to the ratio of the polymer crystalline to amorphous regions. Crystallinity index of BNC is affected by fermentation variables, physiological and nutritional variables, and drying process variables, respectively.[36]

Fig. 6a shows the N_2 adsorption–desorption isotherms obtained through BET analysis. The hysteresis loops confirm the presence of type IV isotherms, commonly linked to mesoporous materials. According to Thommes *et al.* such isotherms represent adsorption behaviour characterized by the gradual formation of monolayers and multilayers on the material's surface, culminating in a marked rise in gas uptake due to capillary condensation within the mesopores.[37] The adsorption process halts upon reaching saturation as all available pores become filled. The pore size distribution of BNC-J, depicted in Fig. 6b, indicates that the majority of pores are concentrated around a pore radius of 15.8 Å, suggesting a relatively narrow pore size distribution and a well-structured mesoporous framework. The measured surface area and pore volume were 89.420 m^2 g^{-1} and 0.225 cc g^{-1}, respectively. These findings are in agreement with earlier reports,[27,38] further validating that BNC exhibits type IV isotherm behaviour and mesoporous characteristics.

The BNC synthesized using WSM as a carbon source exhibited a zeta potential of −30.3 mV, as illustrated in Fig. 6c, indicating its surface charge characteristics and stable colloidal nature. This negative zeta potential aligns with the inherent electronegativity of cellulose and may be attributed to an increase in negatively charged groups formed during mechanical processing.[39] The substantial absolute value suggests that the BNC dispersion maintains good stability in aqueous media, effectively preventing fast particle aggregation. These findings support the feasibility of incorporating BNC into composite filter membranes with ceramic materials and other chemical agents.[40]

3.4. Adsorption mechanisms of 2,4-D and TC on BNC

Fig. 7 shows the proposed mechanism of pollutant adsorption onto BNC. FTIR and FESEM analyses confirmed physical and chemical changes in BNC after adsorption. FESEM images Fig. 8a and b revealed aggregated clusters on BNC fibres, resulting in a coarser surface texture, highlighting effective binding of tetracycline (TC) and 2,4-D. FTIR analysis Fig. 8c showed decreased and broadened O–H stretching vibrations, indicating involvement of hydroxyl groups in adsorption. Particularly, the peak at 1640 cm^{-1} shifted to 1660 cm^{-1} after 2,4-D adsorption, reflecting changes in the molecular environment, while this peak disappeared entirely after TC adsorption, suggesting stronger interactions or saturation of binding sites. These spectral changes indicate the involvement of surface functional groups of BNC in the adsorption process, suggesting adsorption governed primarily by electrostatic interactions and hydrogen bonding between the BNC matrix and the adsorbates. In addition, the presence of aromatic rings in both TC and 2,4-D supports the contribution of π–π interactions, which further enhance adsorption affinity onto the BNC surface.[27]
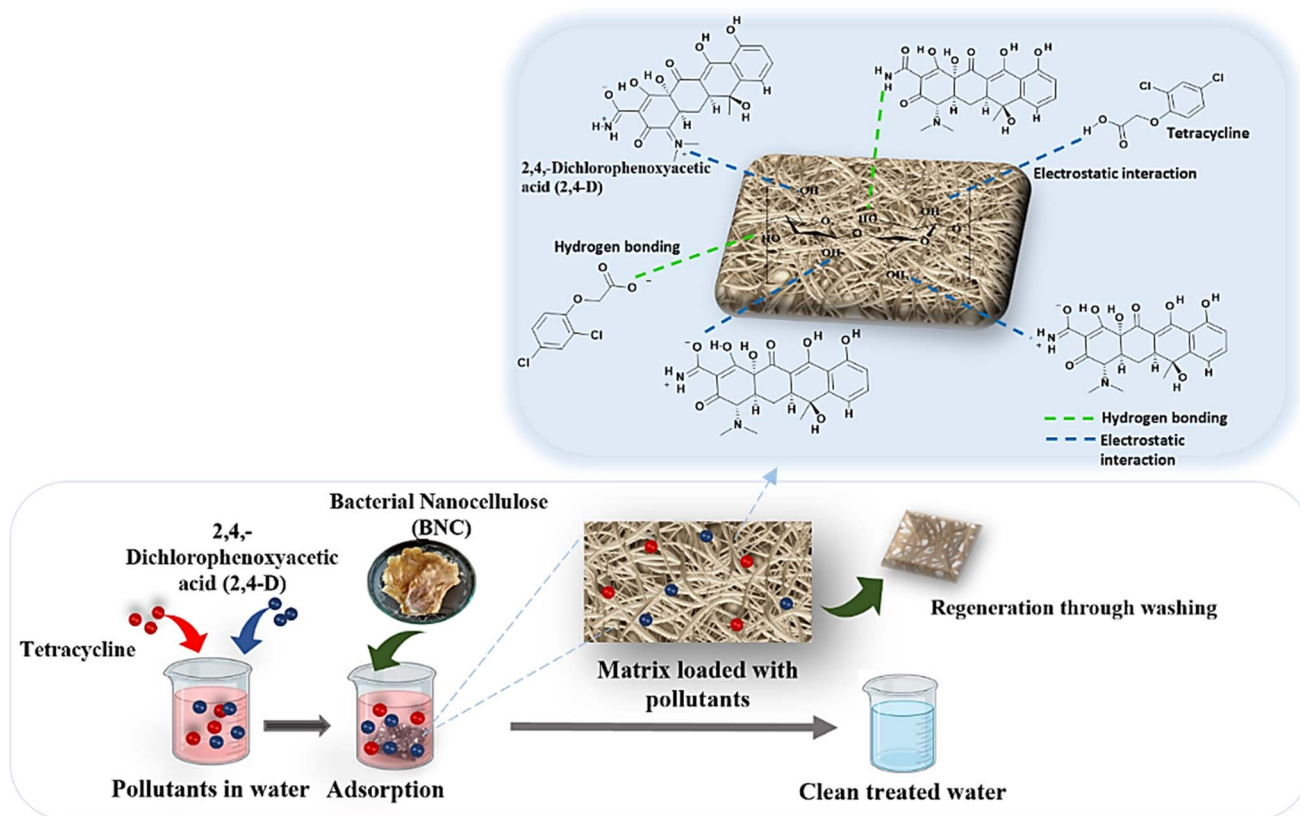

Fig. 7 Adsorption mechanism of the pollutants onto BNC.

Batch experiments were conducted to evaluate the effects of adsorbent dosage, initial pollutant concentration, contact time, pH, and temperature on BNC's adsorption performance. Under optimal conditions, BNC achieved removal efficiencies of 96.42% for TC and 96.23% for 2,4-D using doses of 0.5 g and 0.3 g, respectively Fig. 9a. Beyond these doses, efficiency plateaued, likely due to particle aggregation or overlapping on the BNC surface, which reduces available surface area and increases diffusion paths. Therefore, 0.5 g and 0.3 g were selected for TC and 2,4-D in subsequent tests to balance efficiency and prevent aggregation. Fig. 9 b–c show that for TC, optimal adsorption occurred at 40 mg L^{-1} within 100 minutes, while 2,4-D showed maximum removal at 50 mg L^{-1} in 120 minutes. The differing optimal conditions reflect how each pollutant's chemical structure influences its interaction with the BNC matrix.

pH significantly influences adsorption by altering the charge characteristics of both the adsorbent and the adsorbate. Here, the adsorption behaviour of TC and 2,4-D was examined across a pH range from 3 to 10, with specified conditions including 40 mg L^{-1} for TC and 50 mg L^{-1} for 2,4-D, adsorbent amounts of 0.5 g and 0.3 g, respectively, and contact times of 100 minutes for TC and 120 minutes for 2,4-D at 298 K. The results, shown in Fig. 9d, revealed that TC's adsorption efficiency improved from pH 3 to 7, achieving a peak adsorption of 96.15%. Beyond pH 7, a steady decrease in adsorption was noted. This pattern can be attributed to the different ionic forms of TC under varying pH levels. At low pH, tetracycline predominantly exists in a positively charged cationic form, which enhances its attraction to negatively charged adsorbent surfaces. In the pH range of 5 to 7, TC assumes a zwitterionic form, balancing both positive and negative charges, which allows effective adsorption due to optimal interactions. As pH increases beyond 7, TC shifts to an anionic form, reducing its interaction with the similarly negatively charged adsorbent surface, leading to decreased adsorption efficiency.[41] For 2,4-D, adsorption was most efficient at pH 3, achieving a removal rate of 95.03%. As the solution pH rose, the amount of 2,4-D adsorbed diminished. This trend is consistent with adsorption behaviours on activated carbon, where higher pH levels reduce adsorption capacity due to an increase in electrostatic repulsion between the adsorbate and adsorbent. At higher pH, 2,4-D undergoes greater dissociation, becoming more negatively charged. Consequently, as the solution pH increases, the negatively charged functional groups on the BNC surface repel the increasingly negative 2,4-D molecules, causing a decline in equilibrium adsorption capacity.[42]

Temperature is significant on the process of adsorption since it changes the interaction dynamics between the adsorbate and adsorbent. In this work, the temperature was raised from 298 K to 328 K to see its outcome on the removal efficiency of TC and 2,4-D. The increased temperature greatly enhanced the adsorption capacity of both TC and 2,4-D Fig. 9e. Peak removal efficiencies at the higher temperature of 328 K were recorded to be 97.85% for TC and 97.2% for 2,4-D. This further demonstrates that elevated temperatures promote effective adsorption of these compounds on the adsorbent; hence, temperature is one of the variables of choice for optimization of the adsorption processes for TC and 2,4-D.

3.4.1 Adsorption kinetics modelling. The adsorption kinetics of TC and 2,4-D adsorption onto BNC were examined using two established models: the Lagergren pseudo-first-order model and the Ho pseudo-second-order model. The Lagergren pseudo-first-order (PFO) model, originally proposed by Lagergren[43] is represented by eqn (4):

$$\log (q_e - q_t) = \log q_e - k_1 t \tag{4}$$

The variable k_1 represents the rate constant for the pseudo-first-order, t indicates the duration of contact time, q_e and q_t
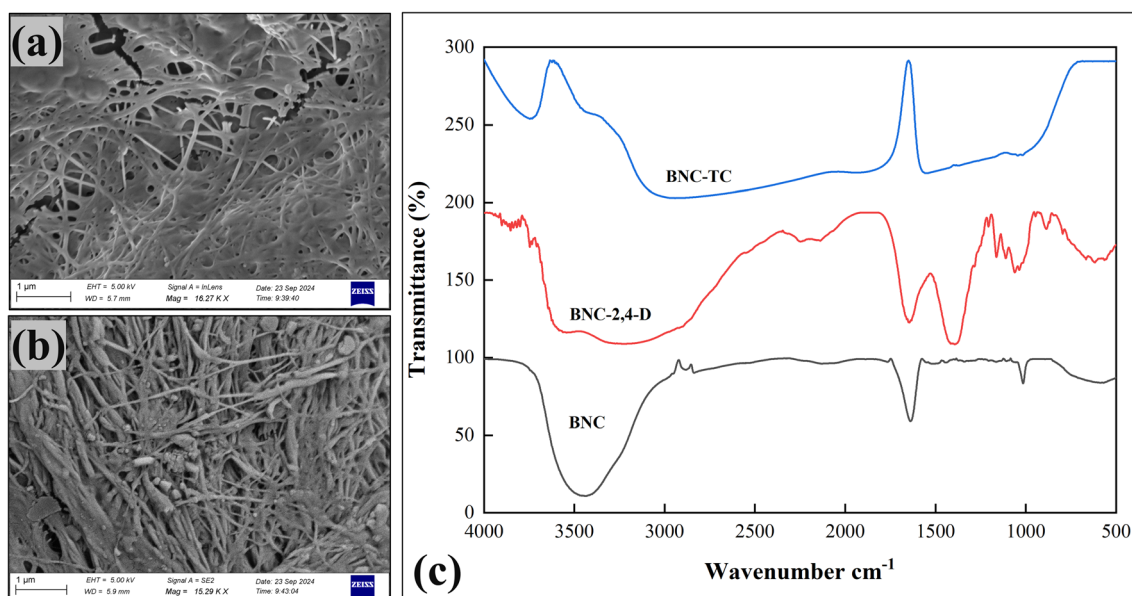

Fig. 8 FE-SEM images of the BNC post-adsorption of (a) TC (magnification = 16.27 kX; scale bar = 1 μm), (b) 2,4-D (magnification = 15.29 kX; scale bar = 1 μm), and (c) FTIR spectrum of pre- and post-adsorption of TC and 2,4-D.
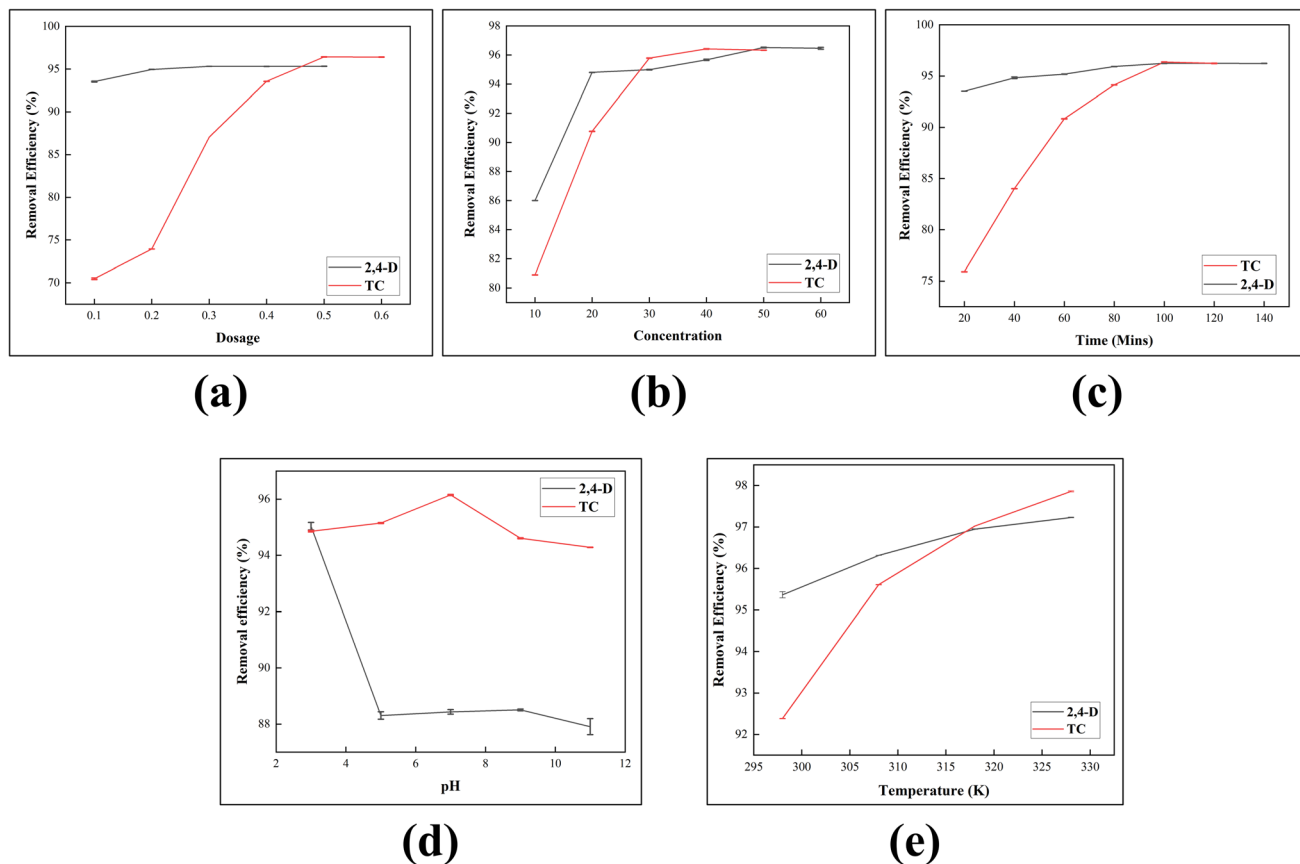
Fig. 9 Effect of (a) dosage (b) initial concentration (c) time (d) pH and (e) temperature on the adsorption of TC and 2,4-D by BNC.

are the amounts of dye (mg g^{-1}) adsorbed at equilibrium and at a given time t (minutes), respectively.

The Ho pseudo-second-order (PSO)[44] kinetic model is shown in eqn (5):

$$\frac{1}{q_t} = \frac{1}{k_2 q_e} + \frac{t}{q_e} \qquad (5)$$

where k_2 is the pseudo-second-order adsorption rate constant, t indicates the duration of contact time, q_e and q_t are the amounts

of dye (mg g^{-1}) adsorbed at equilibrium and at a given time t (minutes), respectively.

The batch kinetic data for adsorption were analyzed by fitting them to both the pseudo-first-order (PFO) and pseudo-second-order (PSO) models using nonlinear methods, as displayed in Fig. 10a–c, with the corresponding kinetic model parameters summarized in Table 3. Both TC and 2,4-D exhibited similar kinetic patterns, with the PSO model providing a better fit. This conclusion is drawn from the higher
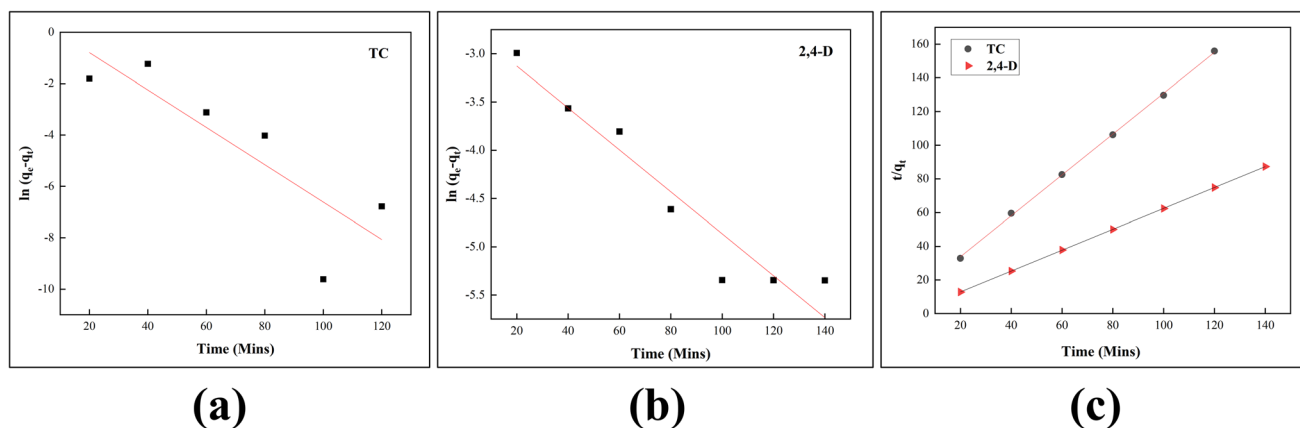
Fig. 10 (a) Pseudo first order of TC, (b) pseudo first order of 2,4-D, and (c) pseudo-second order of TC and 2,4-D.

Table 3 Kinetic parameters for adsorption of TC and 2,4-D onto BNC

Adsorbates	Pseudo-first order	Pseudo-second order
TC	$q_{e(exp)} = 0.771$	$q_{e(exp)} = 0.771$
	$q_{e(cal)} = 1.51$	$q_{e(cal)} = 0.824$
	$k_1 = 0.000727$	$k_2 = 0.07$
	$R^2 = 0.72$	$R^2 = 0.99$
2,4-D	$q_{e(exp)} = 1.608$	$q_{e(exp)} = 1.608$
	$q_{e(cal)} = 0.3713$	$q_{e(cal)} = 1.614$
	$k_1 = 0.00018$	$k_2 = 5.1379$
	$R^2 = 0.91$	$R^2 = 0.99$

correlation coefficients ($R^2 = 0.99$ for TC and $R^2 = 0.99$ for 2,4-D) achieved by the PSO model, as well as the close alignment between observed and predicted q_e values. The superior fit of the PSO model indicates that adsorption rates for TC and 2,4-D are influenced more by the availability of adsorption sites rather than initial concentrations, a core assumption of the PSO model, which aligns with this observed kinetics.[45]

3.4.2 Adsorption isotherm modelling. Three isotherm models, Langmuir, Freundlich, and Temkin models, were considered to illustrate the experimental results. The Langmuir isotherm[46] is given by eqn (6):

$$\text{Langmuir isotherm}: \frac{C_e}{q_e} = \frac{1}{q_{max}K_L} + \frac{1}{q_{max}}C_e \qquad (6)$$

C_e (mg L^{-1}) represents the concentration of the adsorbate in the solution at equilibrium, q_e (mg g^{-1}) represents the amount of adsorbate adsorbed at equilibrium, q_{max} (mg g^{-1}) represents the monolayer adsorption capacity, K_L represents the equilibrium adsorption constant.

The Freundlich isotherm[47] is given by eqn (7):

$$\text{Freundlich isotherm}: \log q_e = \frac{1}{n_F}(\log C_e) + \log K_F \qquad (7)$$

Here K_F represents the Freundlich constant, n represents the intensity of the adsorption, C_e (mg L^{-1}) represents the concentration of the adsorbate in the solution at equilibrium, and q_e (mg g^{-1}) represents the amount of adsorbate adsorbed at equilibrium.

The Temkin isotherm[48] is given by eqn (8):

$$\text{Temkin isotherm}: q_e = \frac{RT}{B_T}\ln(A_T C_e) \qquad (8)$$

Here, the amount of adsorbate adsorbed at equilibrium is denoted by q_e (mg g^{-1}), while C_e (mg L^{-1}) represents the equilibrium concentration of the adsorbate in solution. R is the universal gas constant and T (measured in Kelvin) is the absolute temperature. The constant B_T is related to the heat of adsorption and reflects the effect of indirect adsorbate–adsorbate interactions. A_T (L mg^{-1}) is the Temkin isotherm equilibrium binding constant.

The adsorption isotherms are shown in Fig. 11 a–f, and the corresponding parameters are listed in Table 4. The R^2 values demonstrated that the Langmuir isotherm model more precisely signified the adsorption of TC and 2,4-D on BNC, with

R^2 values of 0.995 and 0.999, respectively. This high level of fit supports the Langmuir model's effectiveness in describing the equilibrium data, potentially as the active sites on the BNC surface are evenly dispersed, aligning with the Langmuir model's assumption of surface uniformity. Comparable findings were observed in reported studies on TC and 2,4-D adsorption onto Fe-based metal–organic frameworks[17] and activated carbon.[42]

3.4.3 Thermodynamic evaluation of the adsorption process. To assess how the temperature influences the adsorption of TC and 2,4-D onto BNC, equilibrium studies were conducted at 298 K, 308 K, and 318 K. The thermodynamic parameters, including standard Gibbs free energy ($\Delta G°$), enthalpy ($\Delta H°$), and entropy ($\Delta S°$) were calculated to gain insight into the nature and mechanism of the adsorption process. $\Delta H°$ and $\Delta S°$ were derived from the slope and intercept of the Van't Hoff plot of ln K_d versus $1/T$ for the highest initial concentration of TC and 2,4-D using the expression given in eqn (9).

$$\ln K_d = \frac{\Delta S°}{R} - \frac{\Delta H°}{RT} \qquad (9)$$

where K_d denotes the dimensionless equilibrium distribution coefficient, R (8.314 J K^{-1}mol^{-1}) denotes the universal gas constant and T (K) denotes the absolute temperature. The values of $\Delta G°$ were calculated from eqn (10).

$$\Delta G° = \Delta H° - T\Delta S° \qquad (10)$$

$$K_d = \frac{q_e}{C_e} \qquad (11)$$

Using eqn (10) and (11), K_d and $\Delta G°$ were determined. K_d represents the distribution coefficient, q_e is the amount of adsorbate retained by the adsorbent per litre of solution at equilibrium, C_e is the equilibrium concentration of the adsorbate in the solution, R denotes the gas constant (8.314 J K^{-1}mol^{-1}), and T is the absolute temperature. $\Delta H°$ and $\Delta S°$ were computed using the graph that plotted ln (K_d) against $1/T$.

The assessed values of the different parameters associated to thermodynamics are shown in Table 5. The adsorption of 2,4-D and TC onto BNC is characterized by positive enthalpy changes ($\Delta H°$), indicating that the process is endothermic and becomes more favourable at elevated temperatures. The negative values of Gibbs free energy ($\Delta G°$) at all temperatures confirm that the adsorption occurs spontaneously and is thermodynamically feasible. This spontaneous nature, combined with BNC's strong interaction with both compounds, likely contributes to its substantial adsorption capacity. Furthermore, the positive entropy changes ($\Delta S°$) reflect an increase in disorder at the interface between the solid adsorbent and the solution, highlighting enhanced molecular mobility and a favourable affinity between BNC and the adsorbates.

3.5. Regeneration studies

During desorption, the release of previously adsorbed molecules modifies the characteristics of the film, as illustrated in
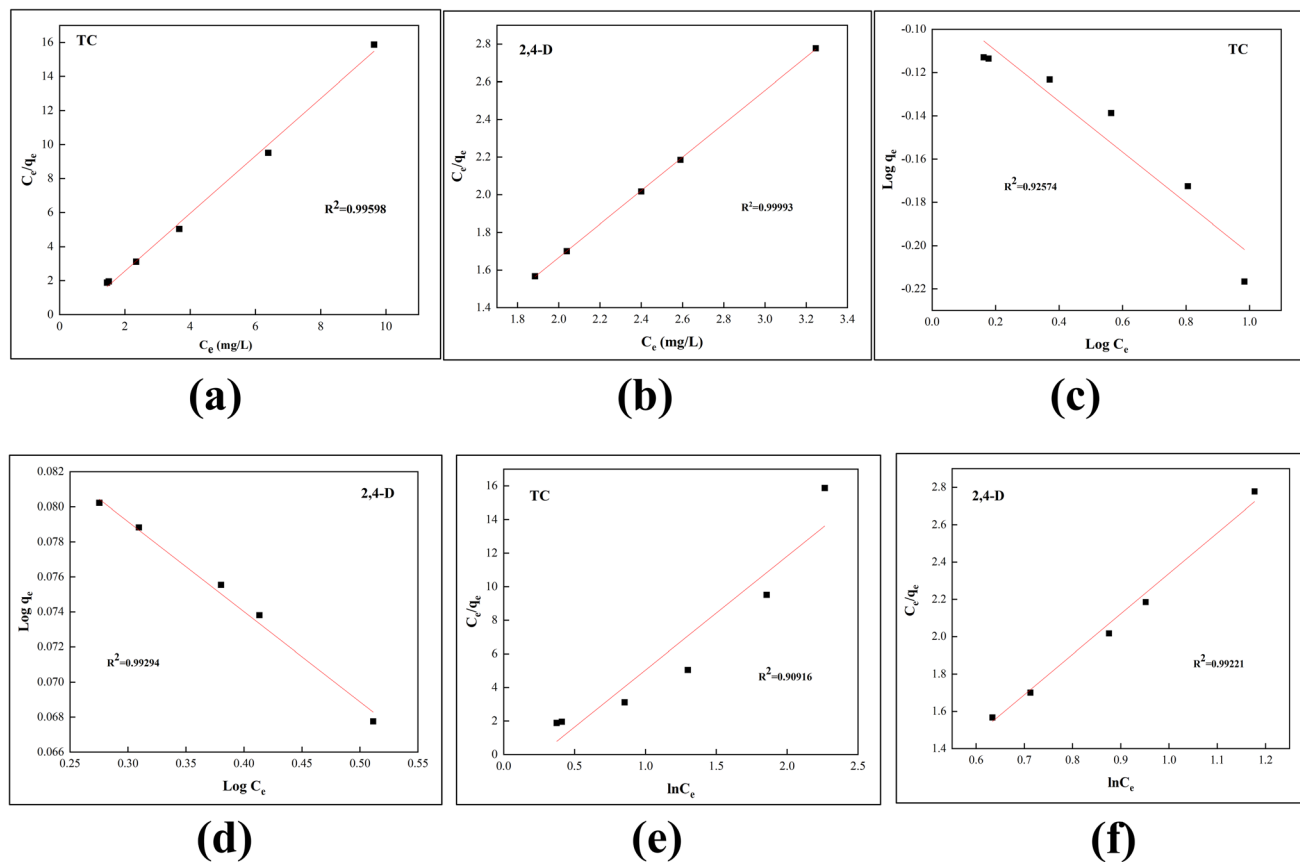
Fig. 11 (a and b) Langmuir, (c and d) Freundlich, and (e and f) Temkin adsorption isotherms of TC and 2,4-D.

Table 4 Adsorption isotherm parameters for the removal of TC and 2,4-D by BNC

Adsorbates	Langmuir	Freundlich	Temkin
TC	$q_{max}\ (\mathrm{mg\ g^{-1}}) = 1.22$	$K_F = 2.44$	$b_T = 6.7869$
	$K_L = 0.072$	$1/n = 8.524$	$K_T = 1.2944$
	$R^2 = 0.995$	$R^2 = 0.92$	$R^2 = 0.90$
2,4-D	$q_{max}\ (\mathrm{mg\ g^{-1}}) = 9.3057$	$K_F = 1.24$	$b_T = 2.16528$
	$K_L = 10.488$	$1/n = 19.447$	$K_T = 1.08344$
	$R^2 = 0.99993$	$R^2 = 0.99294$	$R^2 = 0.99065$

Fig. 12 a–b. The degree where the film's original characteristics can be restored depends on how reversible the adsorption–desorption process is. This process can lead to changes in the surface structure of the adsorbent, including aggregate formation, surface roughening, and other structural changes. Disruptions in the surface molecular arrangement during desorption may result in noticeable alterations to surface

features. To examine the material's effectiveness, BNC was tested through five regeneration cycles under optimized conditions: 40 mg L^{-1} of TC with 0.5 g of adsorbent for 100 minutes, pH 7, and 50 mg L^{-1} of 2,4-D with 0.3 g of adsorbent for 120 minutes, pH 3, all at 328 K. Fig. 12c shows removal efficiency after each cycle, with TC at 88.06% and 2,4-D at 93.55% in the first cycle, gradually decreasing to 75.8% and 85.9% by the fifth. Although results indicate BNC's reusability, a slight reduction in adsorption efficiency was observed after repeated use, likely due to incomplete desorption of TC and 2,4-D by NaOH. These findings suggest BNC's potential as a sustainable adsorbent, but further studies are needed to refine regeneration techniques and boost both adsorptive performance and reusability in practical applications.

3.6. Biodegradation of BNC

Biodegradable materials are typically defined by their capacity to break down naturally within a relatively short timeframe, and

Table 5 Thermodynamic parameters for adsorption of TC and 2,4-D onto BNC

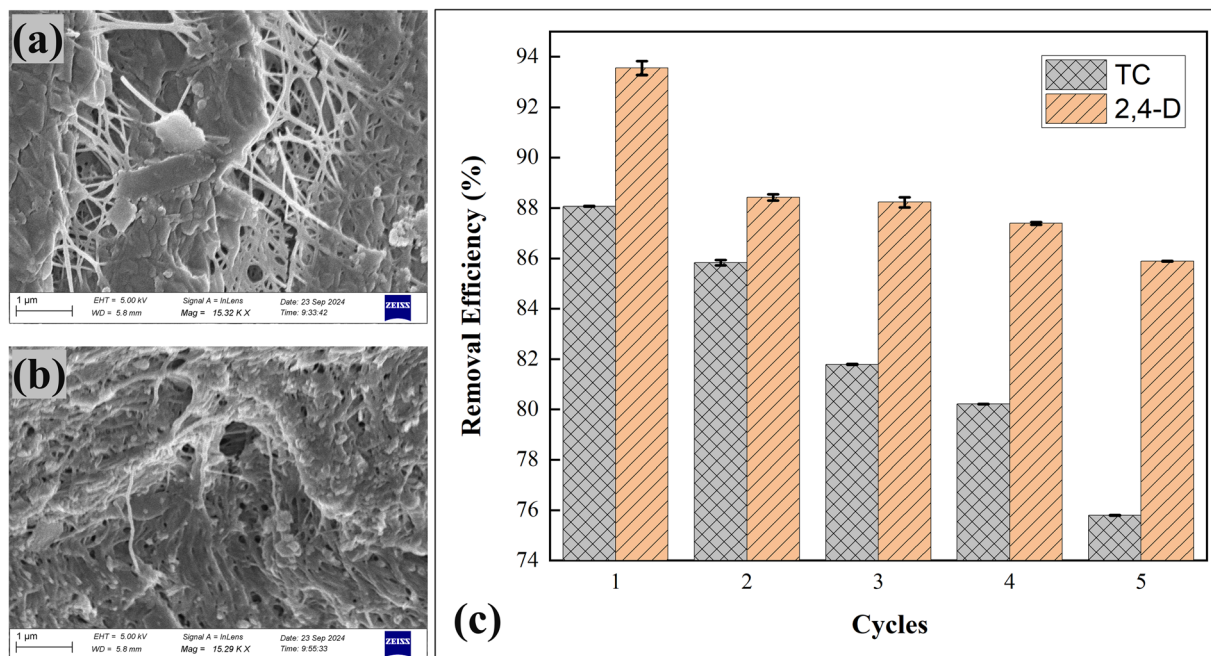| Adsorbate	ΔH° (kJ mol^{-1})	ΔS° (kJ mol^{-1})	ΔG° (kJ mol^{-1}) 298 (K)	308 (K)	318 (K)	328 (K)
TC	35.916	0.10917	−32.5246	−33.6163	−34.708	−35.7997
2,4-D	14.681	0.04633	−13.129	−13.5924	−14.0558	−14.5192

Fig. 12 FESEM of BNC after desorption of (a) TC (Magnification = 15.32 kX; scale bar = 1 μm), (b) 2,4-D (Magnification = 15.29 kX; scale bar = 1 μm), and (c) BNC regeneration cycles.

BNC conforms to this definition due to its hydrophilic structure and strong water absorption capacity.[49] These characteristics facilitate water retention and microbial activity, both of which contribute to the material's gradual disintegration under favorable conditions.[50] The biological factors, especially the presence of microorganisms in the soil, are considered critically important. For instance, certain enzymes produced by fungi, such as *Aspergillus fumigatus*, decompose BNC by severing hydrogen bonds, which accelerates its degradation.[51] Additionally, environmental conditions, particularly those that are wet or have high moisture, contribute to the breakdown of the material by reducing inter-fiber hydrogen bonding and enhancing microbial activity. When BNC comes into contact with soil, these conditions can promote a consistent rate of degradation.[50] In the present study, the biodegradation behaviour of BNC films was evaluated using a soil burial method under ambient environmental conditions, and the extent of biodegradation was quantified based on weight loss over time. This approach simulates a realistic environmental disposal scenario in which biodegradable adsorbent materials are introduced into soil and degraded through the action of native soil microorganisms under natural moisture and temperature
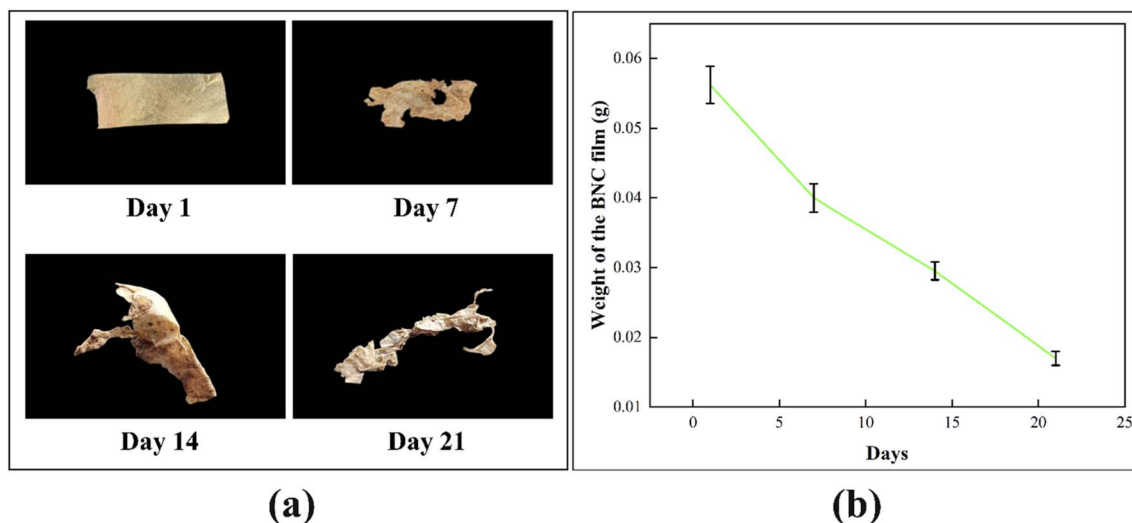

Fig. 13 (a) Morphological changes of BNC film during 21 days of soil burial and (b) changes in weight during 21 days.

Table 6 The amount of weight loss and BNC degradation

Days	Weight of the film (g)	BNC degradation (%)
Day 1	0.056 ± 0.0026	0
Day 7	0.04 ± 0.003	40.58%
Day 14	0.029 ± 0.0012	47.48%
Day 21	0.017 ± 0.001	69.76%

conditions. Fig. 13a shows visible changes in the case of BNC films degrading in soil over time. After 7 days, the films began to exhibit clear signs of change: wrinkling, small holes, and increased degradation led to a major reduction in size and weight. With increasing burial time, the extent of degradation intensified, and after 21 days, only a small portion of the original film remained intact. Based on the weight loss measurements, the BNC films exhibited a biodegradation of approximately 69.7% after 21 days, confirming their biodegradable nature. The soil burial method employed in this study is widely used to assess the environmental degradability of biopolymeric materials and provides a realistic representation of post-use disposal scenarios, where degradation is governed by native soil microorganisms and ambient environmental conditions. The weights of BNC films were also observed and are summarized in Table 6. Fig. 13b shown the weight loss profile following graphical analysis.

4. Conclusion

This research demonstrates the potential of waste sugarcane molasses (WSM) as an eco-friendly carbon source for BNC production by *K. saccharivorans* NUWB1. The resulting BNC exhibited desirable physicochemical properties, including a dense fibril network and high thermal stability, making it suitable for adsorption applications. BNC achieved high removal efficiencies for the herbicide 2,4-D and the antibiotic tetracycline, reaching up to 96.42% and 96.23%, respectively, under optimal conditions. Although five regeneration cycles confirmed BNC's reusability, some efficiency loss suggests further optimization of desorption processes is needed. The BNC's biodegradability, with 69.7% degradation in 21 days, emphasizes its environmental sustainability. Overall, this study highlights BNC produced from agricultural waste as a promising, sustainable solution for managing pollutant-laden agricultural runoff, with opportunities for broader environmental applications pending further research on regeneration and reuse.

Conflicts of interest

The authors declare no conflicts of interest.

Data availability

This manuscript and its additional information files contain all of the data generated or analysed during the study.

Supplementary information (SI) is available. See DOI: https://doi.org/10.1039/d5ra08849f.

References

1 R. Kumar and M. Kumar, Upgradation of jaggery production and preservation technologies, *Renewable Sustainable Energy Rev.*, 2018, **96**, 167–180, DOI: 10.1016/j.rser.2018.07.053.

2 S. Keshk and K. Sameshima, The utilization of sugar cane molasses with/without the presence of lignosulfonate for the production of bacterial cellulose, *Appl. Microbiol. Biotechnol.*, 2006, **72**, 291–296, DOI: 10.1007/s00253-005-0265-6.

3 P. K. Poddar and O. Sahu, Quality and management of wastewater in sugar industry, *Appl. Water Sci.*, 2015, **7**, 461–468, DOI: 10.1007/s13201-015-0264-4.

4 N. Tyagi and S. Suresh, Production of cellulose from sugarcane molasses using *Gluconacetobacter intermedius* SNT-1: optimization & characterization, *J. Cleaner Prod.*, 2016, **112**, 71–80, DOI: 10.1016/j.jclepro.2015.07.054.

5 M. Hasnain, N. Munir, Z. S. Siddiqui, F. Ali, A. El-Keblawy and Z. Abideen, Integral Approach for the Evaluation of Sugar Cane Bio-Waste Molasses and Effects on Algal Lipids and Biodiesel Production, *Waste Biomass Valorization*, 2023, **14**, 23–42, DOI: 10.1007/s12649-022-01864-0.

6 K. Amutha, *Sustainable Chemical Management and Zero Discharges*, Elsevier eBooks, 2017, 347–366.

7 G. Pagliano, V. Ventorino, A. Panico and O. Pepe, Integrated systems for biopolymers and bioenergy production from organic waste and by-products: a review of microbial processes, Biotech, *Biofuels*, 2017, **10**, 113, DOI: 10.1186/s13068-017-0802-4.

8 M. L. Cacicedo, M. C. Castro, I. Servetas, L. Bosnea, K. Boura, P. Tsafrakidou, A. Dima, A. Terpou, A. Koutinas and G. R. Castro, Progress in bacterial cellulose matrices for biotechnological applications, *Bioresour. Technol.*, 2016, **213**, 172–180, DOI: 10.1016/j.biortech.2016.02.071.

9 B. Walling, P. Bharali, B. Giridharan, B. Gogoi, V. Sorhie, Alemtoshi and S. K. Mani, Bacterial nanocellulose: A novel nanostructured bio-adsorbent for green remediation technology, *Acta Ecol. Sin.*, 2023, **43**, 946–967, DOI: 10.1016/j.chnaes.2023.02.002.

10 P. C. Kesavan and S. Malarvannan, Green to evergreen revolution; ecological and evolutionary perspectives in pest management, *Curr. Sci.*, 2010, **99**, 908–914.

11 L. Ding, X. Lu, H. Deng and X. Zhang, Adsorptive Removal of 2,4-Dichlorophenoxyacetic Acid (2,4-D) from Aqueous Solutions Using MIEX Resin, *Ind. Eng. Chem. Res.*, 2012, **51**, 11226–11235, DOI: 10.1021/ie300469h.

12 B. K. Jung, Z. Hasan and S. H. Jhung, Adsorptive removal of 2,4-dichlorophenoxyacetic acid (2,4-D) from water with a metal–organic framework, *Chem. Eng. J.*, 2013, **234**, 99–105, DOI: 10.1016/j.cej.2013.08.110.

13 Y. Xi, M. Mallavarapu and R. Naidu, Adsorption of the herbicide 2,4-D on organo-palygorskite, *Appl. Clay Sci.*, 2010, **49**, 255–261, DOI: 10.1016/j.clay.2010.05.015.

14 X. Chen, X. Liu, L. Zhu, X. Tao and X. Wang, One-step fabrication of novel MIL-53(Fe, Al) for synergistic adsorption-photocatalytic degradation of tetracycline, *Chemosphere*, 2022, **291**, 133032, DOI: 10.1016/j.chemosphere.2021.133032.

15 Q.-X. Zhou, Q.-R. Zhang and T.-H. Sun, Technical Innovation of Land Treatment Systems for Municipal Wastewater in Northeast China, *Pedosphere*, 2006, **16**, 297–303, DOI: 10.1016/S1002-0160(06)60055-6.

16 X. Xie, Q. Zhou, D. Lin, J. Guo and Y. Bao, Toxic effect of tetracycline exposure on growth, antioxidative and genetic indices of wheat (Triticum aestivum L.), *Environ. Sci. Pollut. Res.*, 2010, **18**, 566–575, DOI: 10.1007/s11356-010-0398-8.

17 D. Wang, F. Jia, H. Wang, F. Chen, Y. Fang, W. Dong, G. Zeng, X. Li, Q. Yang and X. Yuan, Simultaneously efficient adsorption and photocatalytic degradation of tetracycline by Fe-based MOFs, *J. Colloid Interface Sci.*, 2018, **519**, 273–284, DOI: 10.1016/j.jcis.2018.02.067.

18 S. Dubey, J. Singh and R. P. Singh, Biotransformation of sweet lime pulp waste into high-quality nanocellulose with an excellent productivity using *Komagataeibacter europaeus* SGP37 under static intermittent fed-batch cultivation, *Bioresour. Technol.*, 2018, **247**, 73–80, DOI: 10.1016/j.biortech.2017.09.089.

19 H. Khan, V. Saroha, S. Raghuvanshi, A. K. Bharti and D. Dutt, Valorization of fruit processing waste to produce high value-added bacterial nanocellulose by a novel strain *Komagataeibacter xylinus* IITR DKH20, *Carbohydr. Polym.*, 2021, **260**, 117807, DOI: 10.1016/j.carbpol.2021.117807.

20 M. Abba, B. B. Nyakuma, Z. Ibrahim, J. B. Ali, S. I. A. Razak and R. Salihu, Physicochemical, Morphological, and Microstructural Characterisation of Bacterial Nanocellulose from *Gluconacetobacter xylinus* BCZM, *J. Nat. Fibers*, 2020, **19**, 4368–4379, DOI: 10.1080/15440478.2020.1857896.

21 B. Walling, A. Borah, S. Hazarika, P. Bharali, D. Ramachandran, V. Kanagasabai, N. Dutta, G. B. Maadurshni, J. Manivannan, P. Mudoi, P. K. Kaman, V. Sorhie, B. Gogoi, Alemtoshi, S. A. Acharjee, V. Vishwakarma and P. D. Nath, Production of bacterial nanocellulose as green adsorbent matrix using distillery wastes for dye removal: a combined approach for waste management and pollution mitigation, *Biomass Convers. Biorefin.*, 2025, **15**, 7265–7281, DOI: 10.1007/s13399-024-05561-x.

22 W. Xu, L. Liang and M. Zhu, Determination of Sugars in Molasses by HPLC Following Solid-Phase Extraction, *Int. J. Food Prop.*, 2014, **18**, 547–557, DOI: 10.1080/10942912.2013.837064.

23 A. Chikhoune, F. Bedjou, S. Oubouzid, R. Boukefoussa, B. Bechri, H. Tarmoul, T. Abdeladim, A. Tounsi, M. Hamitri, S. Chikh and L. Kouadri, Development of Sugar Cane Molasses in Formulations of Madeleines, Mini Croissants, and Buns Incorporated with Interesterified Oil, *J. Chem.*, 2014, **2014**, 936780, DOI: 10.1155/2014/936780.

24 S. D. Zhantlessova, Zh. Khamitkyzy, A. B. Talipova, I. S. Savitskaya and A. S. Kistaubaeyva, Selection and optimization of cultivation conditions for bacterial cellulose producer, *Int. J. Biol. Chem.*, 2022, **15**, 54–63, DOI: 10.26577/ijbch.2022.v15.i1.06.

25 A. C. Rodrigues, A. I. Fontão, A. Coelho, M. Leal, F. A. G. Soares da Silva, Y. Wan, F. Dourado and M. Gama, Response surface statistical optimization of bacterial nanocellulose fermentation in static culture using a low-cost medium, *New Biotechnol.*, 2019, **49**, 19–27, DOI: 10.1016/j.nbt.2018.12.002.

26 D. R. Ruka, G. P. Simon and K. M. Dean, Altering the growth conditions of *Gluconacetobacter xylinus* to maximize the yield of bacterial cellulose, *Carbohydr. Polym.*, 2012, **89**, 613–622, DOI: 10.1016/j.carbpol.2012.03.059.

27 B. Walling, P. Bharali, D. Ramachandran, V. Kanagasabai, N. Dutta, S. Hazarika, G. B. Maadurshni, J. Manivannan, S. Kumari, S. A. Acharjee, B. Gogoi, Alemtoshi, V. Sorhie and V. Vishwakarma, Bacterial valorization of agricultural-waste into a nano-sized cellulosic matrix for mitigating emerging pharmaceutical pollutants: An eco-benign approach, *Int. J. Biol. Macromol.*, 2024, **277**, 133684, DOI: 10.1016/j.ijbiomac.2024.133684.

28 N. E.-A. El-Naggar, A. B. A. Mohammed and S. E. El-Malkey, Bacterial nanocellulose production using Cantaloupe juice, statistical optimization and characterization, *Sci. Rep.*, 2023, **13**, 51, DOI: 10.1038/s41598-022-26642-9.

29 V. Alves, K. de and M. L. Felsner, Green and fast ultrasound-assisted extraction procedures for Fe, Mn, Mg and Ca analysis in cane syrups by FAAS, *J. Food Compos. Anal.*, 2023, **123**, 105495, DOI: 10.1016/j.jfca.2023.105495.

30 Y. Yan, T. Chen, R. Tan, S. Han, X. Zhang, Y. Shen, X. Hu, S. Zhao, D. Qu, L. Chen, N. Wu and G. Wu, In situ production of bacterial nanocellulose-activated carbon composites from pear juice industry wastewater by two new *Komagataeibacter intermedius* and *Komagataeibacter xylinus* isolates for heavy metal removal, *Environ. Technol. Innovation*, 2023, **33**, 103497, DOI: 10.1016/j.eti.2023.103497.

31 H. S. Barud, C. A. Ribeiro, J. Manual, M. S. Crespi and S. José, Younes Messadeq, Kinetic parameters for thermal decomposition of microcrystalline, vegetal, and bacterial cellulose, *J. Therm. Anal. Calorim.*, 2010, **105**, 421–426, DOI: 10.1007/s10973-010-1118-9.

32 R. T. A. Machado, A. B. Meneguin, R. M. Sábio, D. F. Franco, S. G. Antonio, J. Gutierrez, A. Tercjak, A. A. Berretta, S. J. L. Ribeiro, S. C. Lazarini, W. R. Lustri and H. S. Barud, *Komagataeibacter rhaeticus* grown in sugarcane molasses-supplemented culture medium as a strategy for enhancing bacterial cellulose production, *Ind. Crops Prod.*, 2018, **122**, 637–646, DOI: 10.1016/j.indcrop.2018.06.048.

33 G. Gayathri and G. Srinikethan, Bacterial Cellulose production by *K. saccharivorans* BC1 strain using crude distillery effluent as cheap and cost effective nutrient medium, *Int. J. Biol. Macromol.*, 2019, **138**, 950–957, DOI: 10.1016/j.ijbiomac.2019.07.159.

34 F. D. E. Goelzer, P. C. S. Faria-Tischer, J. C. Vitorino, M.-R. Sierakowski and C. A. Tischer, Production and characterization of nanospheres of bacterial cellulose from

Acetobacter xylinum from processed rice bark, *Mater. Sci. Eng., C*, 2009, **29**, 546–551, DOI: 10.1016/j.msec.2008.10.013.

35 M. Wada, T. Okano and J. Sugiyama, Allomorphs of native crystalline cellulose I evaluated by two equatorial-spacings, *J. Wood Sci.*, 2001, **47**, 124–128, DOI: 10.1007/BF00780560.

36 S. Park, J. O. Baker, M. E. Himmel, P. A. Parilla and D. K. Johnson, Cellulose crystallinity index: measurement techniques and their impact on interpreting cellulase performance, *Biotechnol. Biofuels*, 2010, **3**, 10, DOI: 10.1186/1754-6834-3-10.

37 M. Thommes, R. Guillet-Nicolas and K. A. Cychosz, Physical Adsorption Characterization of Mesoporous Zeolites, *Mesoporous Zeolites: Prep, Charact. Appl.*, 2015, 349–384, DOI: 10.1002/9783527673957.ch11.

38 G. M. de Paiva, L. F. de Melo, F. P. Pedroso, P. da L. Mesquita, E. R. Nucci and I. J. B. Santos, Use of brewer's residual yeast for production of bacterial nanocellulose with *Gluconacetobacter hansenii*, *Int. J. Biol. Macromol.*, 2023, **242**, 124897, DOI: 10.1016/j.ijbiomac.2023.124897.

39 S.-O. Dima, D.-M. Panaitescu, C. Orban, M. Ghiurea, S.-M. Doncea, R. Fierascu, C. Nistor, E. Alexandrescu, C.-A. Nicolae, B. Trică, A. Moraru and F. Oancea, Bacterial Nanocellulose from Side-Streams of Kombucha Beverages Production: Preparation and Physical-Chemical Properties, *Polymers*, 2017, **9**, 374, DOI: 10.3390/polym9080374.

40 E. K. Sijabat, A. Nuruddin, P. Aditiawati and B. S. Purwasasmita, Synthesis and Characterization of Bacterial Nanocellulose from Banana Peel for Water Filtration Membrane Application, *J. Phys.: Conf. Ser.*, 2019, **1230**, 012085, DOI: 10.1088/1742-6596/1230/1/012085.

41 Y. Gao, Y. Li, L. Zhang, Z. Kang, J. Hu, A. Shah and X. Su, Adsorption and removal of tetracycline antibiotics from aqueous solution by graphene oxide, *J. Colloid Interface Sci.*, 2012, **368**, 540–546, DOI: 10.1016/j.jcis.2011.11.015.

42 J. M. Salman, V. O. Njoku and B. H. Hameed, Batch and fixed-bed adsorption of 2,4-dichlorophenoxyacetic acid onto oil palm frond activated carbon, *Chem. Eng. J.*, 2011, **174**, 33–40, DOI: 10.1016/j.cej.2011.08.024.

43 S. K. Lagergren, About the Theory of So-Called Adsorption of Soluble Substances, *Sven. Vetenskapsakad. Handl.*, 1898, **24**, 1–39.

44 Y. S. Ho and G. McKay, Pseudo-second order model for sorption processes, *Process Biochem.*, 1999, **34**, 451–465.

45 W. Rudzinski and W. Plazinski, On the applicability of the pseudo-second order equation to represent the kinetics of adsorption at solid/solution interfaces: a theoretical analysis based on the statistical rate theory, *Adsorption*, 2009, **15**, 181–192, DOI: 10.1007/s10450-009-9167-8.

46 I. Langmuir, The adsorption of gases on plane surfaces of glass, mica and platinum, *J. Am. Chem. Soc.*, 1918, **40**, 1361–1403.

47 H. M. Freundlich, Over the Adsorption in Solution, *J. Phys. Chem.*, 1905, **57**, 385–470.

48 M. I. Temkin, Adsorption Equilibrium and the Kinetics of Processes on Nonhomogeneous Surfaces and in the Interaction between Adsorbed Molecules, *Zh. Fiz. Khim.*, 1940, **15**, 296–332.

49 S. Torgbo and P. Sukyai, Biodegradation and thermal stability of bacterial cellulose as biomaterial: The relevance in biomedical applications, *Polym. Degrad. Stab.*, 2020, **179**, 109232, DOI: 10.1016/j.polymdegradstab.2020.109232.

50 P. Dederko-Kantowicz, A. Sommer and H. Staroszczyk, Structural changes of bacterial cellulose due to incubation in conditions simulating human plasma in the presence of selected pathogens, *Carbohydr. Polym.*, 2021, **266**, 118153, DOI: 10.1016/j.carbpol.2021.118153.

51 M. S. A. Camargo, A. P. Cercal, V. F. Silveira, K. C. B. Mancinelli, R. M. M. Gern, M. C. F. Garcia, G. P. Apati, A. L. dos Santos Schneider and A. P. T. Pezzin, Evaluation of Wet Bacterial Cellulose Degradation in Different Environmental Conditions, *Macromol. Symp.*, 2020, **394**, 2000149, DOI: 10.1002/masy.202000149.